nature COMMUNICATIONS

ARTICLE

DOI: 10.1038/s41467-017-00699-x OPEN

Tricritical wings and modulated magnetic phases in $LaCrGe_3$ under pressure

Udhara S. Kaluarachchi[1,2], Sergey L. Bud'ko[1,2], Paul C. Canfield[1,2] & Valentin Taufour[1,3]

Experimental and theoretical investigations on itinerant ferromagnetic systems under pressure have shown that ferromagnetic quantum criticality is avoided either by a change of the transition order, becoming of the first order at a tricritical point, or by the appearance of modulated magnetic phases. In the first case, the application of a magnetic field reveals a wing-structure phase diagram as seen in itinerant ferromagnets such as $ZrZn_2$ and UGe_2. In the second case, no tricritical wings have been observed so far. Here, we report on the discovery of wing-structure as well as the appearance of modulated magnetic phases in the temperature-pressure-magnetic field phase diagram of $LaCrGe_3$. Our investigation of $LaCrGe_3$ reveals a double-wing structure indicating strong similarities with $ZrZn_2$ and UGe_2. But, unlike these simpler systems, $LaCrGe_3$ also shows modulated magnetic phases similar to CeRuPO. This finding provides an example of an additional possibility for the phase diagram of metallic quantum ferromagnets.

[1] The Ames Laboratory, US Department of Energy, Iowa State University, Ames, IA 50011, USA. [2] Department of Physics and Astronomy, Iowa State University, Ames, IA 50011, USA. [3] Present address: Department of Physics, University of California, Davis, CA 95616, USA. Correspondence and requests for materials should be addressed to P.C.C. (email: canfield@ameslab.gov) or to V.T. (email: vtaufour@ucdavis.edu)

Suppressing a second-order, magnetic phase transition to zero temperature with a tuning parameter (pressure, chemical substitutions, magnetic field) has been a very fruitful way to discover many fascinating phenomena in condensed matter physics. In the region near the putative quantum critical point (QCP), superconductivity has been observed in antiferromagnetic[1] as well as ferromagnetic (FM) systems[2–4]. One peculiarity of the clean FM systems studied so far is that the nature of the paramagnetic-ferromagnetic (PM-FM) phase transition always changes before being suppressed to zero temperature[5]: in most cases, the transition becomes of the first order[6–11]. Recently, another possibility, where a modulated magnetic phase (AFM_Q) appears (spin-density wave, antiferromagnetic order), has been observed in CeRuPO[12, 13], MnP[14, 15], and $LaCrGe_3$[16].

Several theories have been developed to explain those possibilities[17–26]. When a FM transition becomes of the first order at a tricritical point (TCP) in the temperature T pressure p plane, the application of a magnetic field H along the magnetization axis reveals a wing structure phase diagram in the T-p-H space[20, 27]. This is seen in UGe_2[28, 29] and $ZrZn_2$[30] and is schematically represented in Fig. 1a. This phase diagram shows the possibility of a different kind of quantum criticality at the quantum wing critical point (QWCP). In contrast with the conventional QCP, symmetry is already broken by the magnetic field at a QWCP. In the more recently considered case where the transition changes to a AFM_Q phase, no wing structure phase diagram has been reported, but it is found that the AFM_Q is suppressed by moderate magnetic field[12, 13]. This second possible T-p-H phase diagram has been schematically presented in a recent review[5] and reproduced in Fig. 1b.

Here, we report electrical resistivity measurements on $LaCrGe_3$ under pressure and magnetic field. We determine the T-p-H phase diagram and find that it corresponds to a third possibility where tricritical wings emerge in addition to the AFM_Q phase. This type of phase diagram is illustrated in Fig. 1c: it includes both the tricritical wings and the AFM_Q phase. In addition, the phase diagram of $LaCrGe_3$ shows a double wing structure similar to what is observed in the itinerant ferromagnets UGe_2[31] and $ZrZn_2$[32], but with the additional AFM_Q phase. $LaCrGe_3$ is the first example showing such a phase diagram.

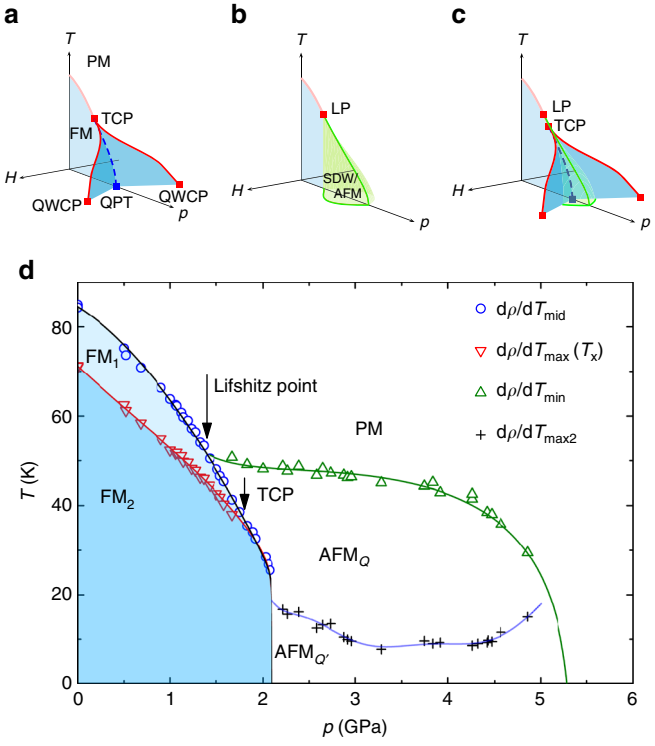

Fig. 1 Temperature–pressure phase diagram. **a** Schematic T-p-H phase diagram of a quantum ferromagnet: the paramagnetic-ferromagnetic (PM-FM) transition becomes of the first order at a tricritical point (TCP) after which there is a quantum phase transition (QPT) at 0 K. Tricritical wings emerge from the TCP under magnetic field and terminate at quantum wing critical points (QWCP). **b** Schematic T-p-H phase diagram of a quantum ferromagnet when a modulated magnetic phase (SDW/AFM) emerges from the Lifshitz point (LP). **c** New possible schematic T-p-H phase diagram for which tricritical wings as well as a new magnetic phase are observed. **d** T-p phase diagram of $LaCrGe_3$ from electrical resistivity measurements[16] showing two FM regions (FM1 and FM2) separated by a crossover. The *solid lines* are guides to the eye

Results

***T*-*p* phase diagram**. Recently, we reported on the T-p phase diagram of $LaCrGe_3$[16], which is reproduced in Fig. 1d. At ambient pressure, $LaCrGe_3$ orders ferromagnetically at $TC = 86$ K. Under applied pressure, TC decreases and disappears at 2.1 GPa. Near 1.3 GPa, there is a Lifshitz point[33] at which a new transition line appears. The transition corresponds to the appearance of a modulated magnetic phase (AFM_Q) and can be tracked up to 5.2 GPa. Muon-spin rotation (μSR) measurements show that the AFM_Q phase has a similar magnetic moment as the FM phase but without net macroscopic magnetization[16]. In addition, band structure calculations suggest that the AFM_Q phase is characterized by a small wave-vector Q and that several small Q phases are nearly degenerate. Below the PM-AFM_Q transition line, several anomalies marked as gray cross in Fig. 1d can be detected in $\rho(T)$[16]. These other anomalies within the AFM_Q phase are compatible with the near degeneracy of different Q-states (shown as AFM_Q and $AFM_{Q'}$) with temperature and pressure driven transitions between states with differing wavevectors.

In this article, we determine the three dimensional T-p-H phase diagram of $LaCrGe_3$ by measuring the electrical resistivity of single crystals of $LaCrGe_3$ under pressure and magnetic field.

FM1 and FM2 phases. Whereas most of the features in Fig. 1d were well understood in ref. [16], we also indicate the pressure dependence of T_x ($d\rho/dT_{max}$) at which a broad maximum is observed in $d\rho/dT$ below TC and shown as orange triangles in Fig. 1d. At ambient pressure, $T_x \approx 71$ K. No corresponding anomaly can be observed in magnetization[16], internal field[16] or specific heat[34]. Under applied pressure, T_x decreases and cannot be distinguished from TC ($d\rho/dT_{mid}$) above 1.6 GPa. As will be shown, application of magnetic field allows for a much clearer appreciation and understanding of this feature.

Figure 2a shows the anomalies at T_x and T_C observed in the electrical resistivity and its temperature derivative at 1.14 GPa. For comparison, Fig. 2b shows ambient pressure data for UGe_2[28] where a similar anomaly at T_x can be observed. In UGe_2, this anomaly was studied intensively[35–37]. It corresponds to a crossover between two ferromagnetic phases FM1 and FM2 with different values of the saturated magnetic moment[35, 36]. Under pressure, there is a critical point at which the crossover becomes a first-order transition, which eventually vanishes where a maximum in superconducting-transition temperature is observed[2]. In the case of $LaCrGe_3$, we cannot locate where the crossover becomes a first order transition, since the anomaly merges with the Curie temperature anomaly near 1.6 GPa, very close to the TCP. However, as we will show below, the two transitions can be separated again with applied magnetic field

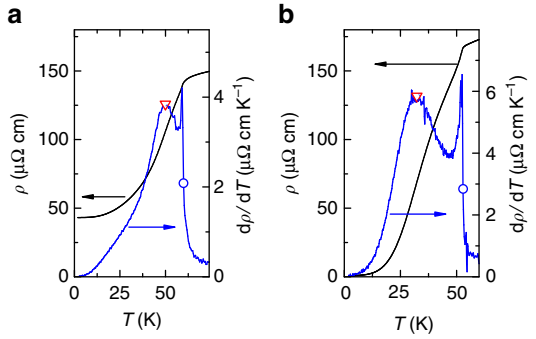

Fig. 2 Comparison of $\rho(T)$ and its $d\rho(T)/dT$ between $LaCrGe_3$ and UGe_2. Temperature dependence of the resistivity (*black line*, *left axis*) and its derivative (*blue line*, *right axis*) of **a** $LaCrGe_3$ at 1.14 GPa and **b** UGe_2 at 0 GPa from ref. [28]. The crossover between the two ferromagnetic phases (FM1 and FM2) is inferred from the maximum in $d\rho/dT$ (T_x) and marked by a *red triangle*, whereas the paramagnetic-ferromagnetic transition is inferred from the middle point of the sharp increase in $d\rho/dT$ (*TC*) and indicated by a *blue circle*

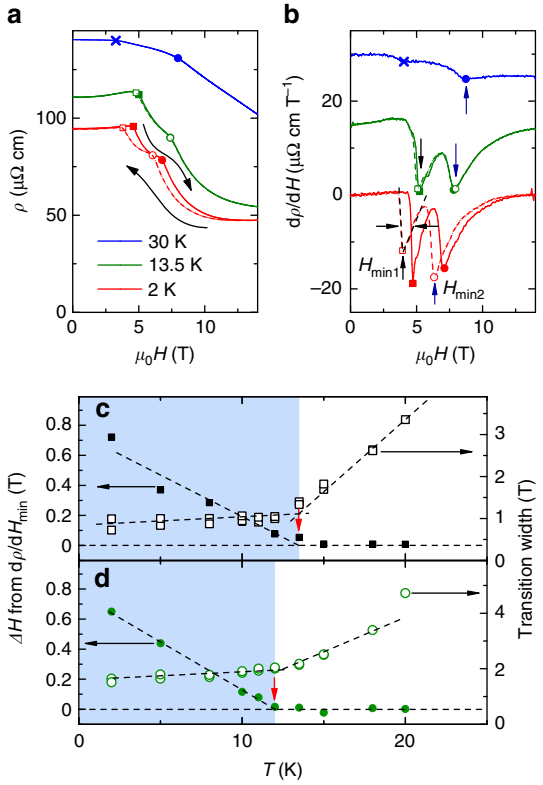

Fig. 3 Determination of wing critical point at 2.39 GPa. **a** Field dependence of the electrical resistivity at 2, 13.5, and 30 K at 2.39 GPa with applied field along the *c*-axis. *Continuous* and *dashed lines* represent the field increasing and decreasing, respectively. When the *continuous* and *dashed lines* do not overlap, there is indication for hysteresis. **b** Corresponding field derivatives ($d\rho/dH$). The curves are shifted by 15 μΩ cm T^{-1} for clarity. *Vertical arrows* represent the minima. The transition width is determined by the full width at half minimum as represented by *horizontal arrows*. *Solid* and *open symbols* in **a**, **b** represent the transition fields for field increasing and decreasing (*squares* for AFM_Q-FM1 and *circles* for FM1-FM2). The *blue cross symbols* in **a**, **b** represent the AFM_Q-PM transition at this pressure. The temperature dependence of the hysteresis width of H_{min1} and H_{min2} (*solid symbols*) are shown in **c**, **d** (*left axes*). The hysteresis width gradually decreases with increasing temperature and disappears at *Tw* corresponding to the wing critical point (*vertical red arrows*). The *right axes* show the temperature dependence of the transition widths (*open symbols*). *Dashed lines* are guides to the eye. The width is small for the first-order transition and becomes broad in the crossover region. The *blue-color shaded area* represents the first order transition region, whereas the *white color area* represents the crossover region. These allow for the determination of the wing critical point of the FM1 transition at 13.5 ± 1.5 K, 2.39 GPa, and 5.1 T and the one for the FM2 transition at 12 ± 1 K, 2.39 GPa and 7.7 T

above 2.1 GPa. This is similar to what is observed in UGe_2 where the PM-FM1 and FM1-FM2 transition lines separate more and more as the pressure and the magnetic field are increased. Because of such similarities with UGe_2, we label the two phases FM1 and FM2 and assume that the anomaly at T_x corresponds to a FM1-FM2 crossover. A similar crossover was also observed in $ZrZn_2$[32]. In refs [18, 25], a Stoner model with two peaks in the density of states near the Fermi level was proposed to account for the two phases FM1 and FM2, reinforcing the idea of the itinerant nature of the magnetism in $LaCrGe_3$.

Field-dependent resistivity measurement under pressure. In zero field, for applied pressures above 2.1 GPa, both FM1 and FM2 phases are suppressed. Upon applying a magnetic field along the *c*-axis, two sharp drops of the electrical resistivity can be observed (Fig. 3a) with two corresponding minima in the field derivatives (Fig. 3b). At 2 K, clear hysteresis of $\Delta H \sim 0.7$ T can be observed for both anomalies indicating the first order nature of the transitions. The emergence of field-induced first-order transitions starting from 2.1 GPa and moving to higher field as the pressure is increased (Supplementary Note 1) is characteristic of the FM quantum phase transition: when the PM-FM transition becomes of the first order, a magnetic field applied along the magnetization axis can induce the transition resulting in a wing structure phase diagram such as the one illustrated in Fig. 1a. In the case of $LaCrGe_3$, evidence for a first order transition was already pointed out because of the very steep pressure dependence of T_C near 2.1 GPa and the abrupt doubling of the residual ($T = 2$ K) electrical resistivity[16]. In UGe_2 or $ZrZn_2$, the successive metamagnetic transitions correspond to the PM-FM1 and FM1-FM2 transitions. In $LaCrGe_3$, at 2 K, due to the presence of the $AFM_{Q'}$ phase at zero field, the transitions correspond to $AFM_{Q'}$-FM1 and FM1-FM2.

Determination of the wing structure phase diagram. As the temperature is increased, the hysteresis decreases for both transitions, as can be seen in Fig. 3c, d and disappears at a wing critical point (WCP). Also, the transition width is small and weakly temperature dependent below the WCP and it broadens when entering in the crossover regime. Similar behavior has been observed in UGe_2[29]. At 2.39 GPa for example, we locate the WCP of the first-order FM1 transition around 13.5 K and the one of the first-order FM2 transition around 12 K. At this temperature and pressure, the transitions occur at 5.1 and 7.7 T, respectively. This allows for the tracking of the wing boundaries in the *T*-*p*-*H* space up to our field limit of 14 T. At low field, near the TCP, the wing boundaries are more conveniently determined as the location of the largest peak in $d\rho/dT$ (Supplementary Note 2).

The projections of the wings lines $T_w(p, H)$ in the *T*-*H*, *T*-*p*, and *H*-*p* planes are shown in Fig. 4a–c, respectively. The metamagnetic transitions to FM1 and FM2 start from 2.1 GPa and separate in the high field region as the pressure is further increased. For the FM1 wing, the slope dT_w/dH_w is very steep near $H = 0$ (Fig. 4a), whereas dH_w/dp_w is very small (Fig. 4c). This is in agreement with a recent theoretical analysis based on the Landau expansion of the free energy, which shows that dT_w/dH_w and dp_w/dH_w are infinite at the TCP[27]. This fact was overlooked

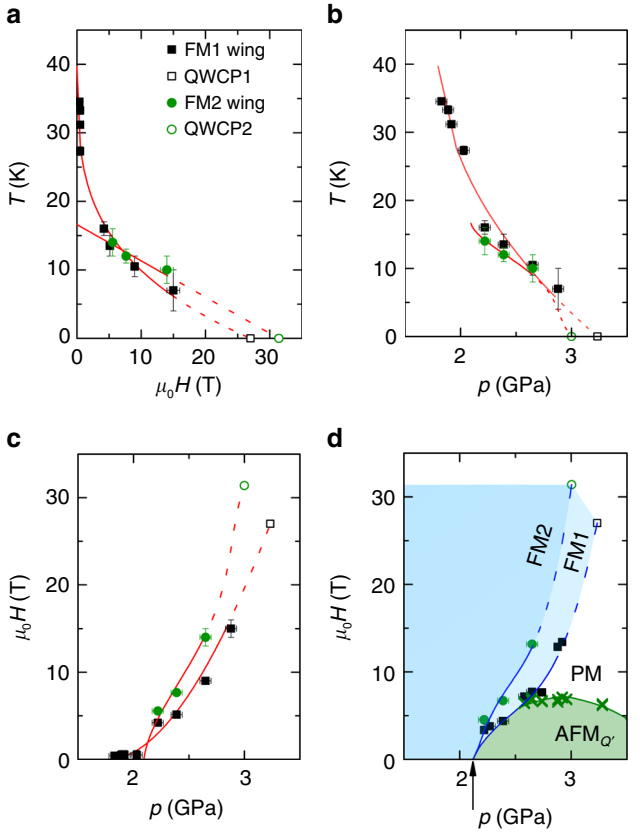

Fig. 4 Shape of the tricritical wing lines (T_w, p_w, H_w). Projection of the wings in **a** *T-H*, **b** *T-p* and **c** *H-p* planes. *Black solid squares* and *green solid circles* represent the FM1-wing and FM2-wing, respectively. *Red lines* (represented in the *T-p-H* space in Fig. 5) are guides to the eyes and *open symbols* represent the extrapolated quantum wing critical point (QWCP). **d** *H-p* phase diagram at 2 K. The *arrow* represents the pressure $p_c = 2.1$ GPa. The *green color cross symbols* represent the $AFM_{Q'}$ phase boundary. *Dark blue*, *light blue*, and *green color shaded areas* represent the FM2, FM1, and $AFM_{Q'}$ phases, respectively. The *error bars* in pressure for **b**–**d** are determined by the superconducting transition width of the Pb manometer. For **a**–**d**, the *error bars* in temperature and magnetic field are determined as half the data spacing

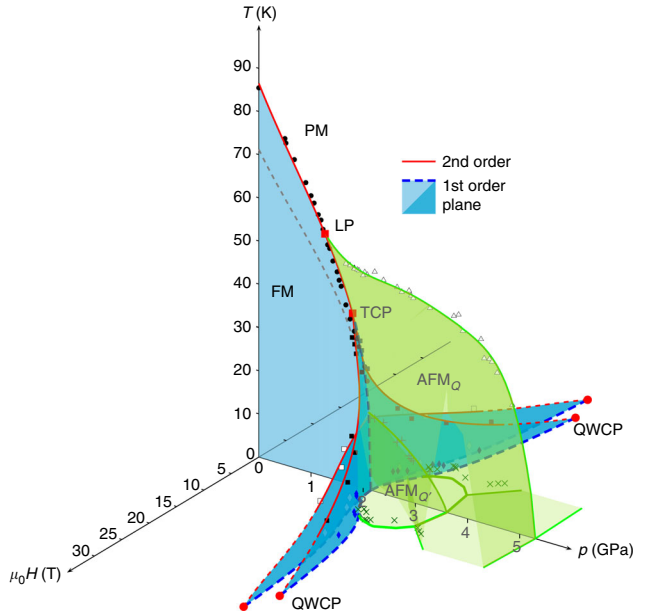

Fig. 5 *T-p-H* phase diagram of $LaCrGe_3$. *Red solid lines* are the second order phase transition and *blue color planes* are planes of first order transitions. *Green color areas* represent the AFM_Q and $AFM_{Q'}$ phases. For clarity, only data points at 2 K and along the transitions lines are shown. *Black circles* indicate the paramagnetic (PM)-ferromagnetic (FM) transition. *Black squares* indicate the wing critical line for FM1 and *empty squares* indicate the wing critical line for FM2. *Blue diamonds* indicate the first order transition to the FM1 state at 2 K and *empty diamonds*, the first order transition to FM2 at 2 K. *Empty triangles* indicate the PM-modulated magnetic phase (AFM_Q) and "+" indicate the $AFM_{Q'}$ boundary. "×" indicate the AFM_Q or $AFM_{Q'}$ boundary at 2 K. The full set of data points can be found in Supplementary Note 3. For clarity, the *green surfaces* representing the boundaries for the AFM_Q or $AFM_{Q'}$ phases are shown only in the region of positive magnetic field

in the previous experimental determinations of the wing structure phase diagram in UGe_2[28, 29] and $ZrZn_2$[30], but appears very clearly in the case of $LaCrGe_3$. In the low field region, there are no data for the FM2 wing since the transition is not well separated from the FM1 wing, but there is no evidence for an infinite slope near $H = 0$. The wing lines can be extrapolated to QWCPs at 0 K in high magnetic fields of the order of ~30 T (Fig. 4a) and pressures around ~3 GPa (Fig. 4b).

Figure 4d shows the *H-p* phase diagram at low temperature ($T = 2$ K). The magnetic field at the transition to the FM1 phase increases rapidly, whereas the field suppressing the $AFM_{Q'}$ phase does not exceed 7 T. Above 2.5 GPa, the $AFM_{Q'}$ and FM1 phases are separated by a region corresponding to the polarized PM phase. We note that a similar diagram where the wings extend beyond the AFM phase was recently obtained theoretically in the case of strong quantum fluctuations effects[38]. The similarity of the *H-p* phase diagram at 2 K (Fig. 4d) and the projection of the wings in the *H-p* plane (Fig. 4c) reveals the near vertical nature of the wings.

***T-p-H* phase diagram of $LaCrGe_3$.** The resulting three-dimensional *T-p-H* phase diagram of $LaCrGe_3$ is shown in Fig. 5, which summarizes our results (Several of the constituent *T-H* phase diagrams, at various pressures, are given in Supplementary Fig. 3). The double wing structure is observed in addition to the AFM_Q phase. This is the first time that such a phase diagram is reported. Other materials suggested that there is either a wing structure without any additional magnetic phase[28–30], or a magnetic phase without a wing structure[12, 13]. The present study illustrates a third possibility where all such features are observed. The phase diagram of $LaCrGe_3$ and the existence of wings clearly establish that the quantum phase transition from FM to $AFM_{Q'}$ is of the first order. It is plausible that the reason is the same as for the FM to PM transition, but no theory is available for this case, as pointed out in a recent review[5]. Another interesting aspect is the existence of the two metamagnetic transitions (to FM1 and FM2) which suggests that this might be a generic feature of itinerant ferromagnetism. Indeed, it is observed in $ZrZn_2$, UGe_2, and $LaCrGe_3$, although these are very different materials with different electronic orbitals giving rise the the magnetic states. We note that a wing structure has also been determined in the PM compounds UCoAl[39–41] and $Sr_3Ru_2O_7$[42], implying that a FM state probably exists at negative pressures in these materials. Strikingly, two anomalies could be detected upon crossing the wings in UCoAl (two kinks of a plateau in electrical resistivity[39], two peaks in the ac susceptibility[41]), as well as in $Sr_3Ru_2O_7$ (two peaks in the ac susceptibility[42]). These double features could also correspond to a double wing structure.

Conclusions. To conclude, the *T-p-H* phase diagram of $LaCrGe_3$ provides a distinct example of possible outcomes of FM quantum

criticality. At zero field, quantum criticality is avoided by the appearance of a new modulated magnetic phase, but the application of magnetic field shows the existence of a wing structure phase diagram leading towards QWCP at high field. These experimental findings reveal insights into the possible phase-diagrams of FM systems. The emergence of the wings reveals a theoretically predicted tangent slope[27] near the TCP, a fact that was overlooked in previous experimental determination of phase diagrams of other compounds because of the lack of data density in that region. In addition, the double nature of the wings appears to be a generic feature of itinerant ferromagnetism, as it is observed in several, a priori, unrelated materials. This result deserves further theoretical investigations and unification.

Methods

Sample preparation. Single crystals of $LaCrGe_3$ were grown using a high-temperature solution growth technique[43, 44]. A mixture of La, Cr, and Ge with a molar ratio of La:Cr:Ge = 13:13:74 was premixed by arc melting. The material was then placed in a 2-mL alumina crucible and sealed in a silica ampoule under partial pressure of high purity argon gas. The sealed ampoule was heated to 1100 °C over 3 h and held for 5 h. After that, it was cooled to 825 °C and the remaining liquid was decanted using a centrifuge. Details about the crystal growth procedure and sample characterization at ambient pressure is described in ref. [34].

The resistivity measurements under pressure. The samples for the pressure study were selected after ambient pressure characterization by the magnetization and resistivity measurements. Temperature and field dependent resistance measurements were carried out using a Quantum Design Physical Property Measurement System from 1.8 to 300 K. The resistivity was measured by the standard four-probe method with the current in the *ab* plane. Four Au wires with diameter of 12.5 µm were spot welded to the sample. A magnetic field, up to 9 or 14 T, was applied along the *c*-axis, which corresponds to the magnetization easy axis[34, 45].

Two types of pressure cells were used for this experiment. A Be-Cu/Ni-Cr-Al hybrid piston-cylinder cell, similar to the one described in ref. [46], was used for pressures up to 2.1 GPa. A mixture of 4:6 light mineral oil: *n*-pentane[46] used as a pressure medium, which solidifies at ~3–4 GPa at room temperature[47]. For higher pressures, a modified Bridgman cell[48] was used to generate pressure up to 6 GPa. A 1:1 mixture of *n*-pentane:iso-pentane was used as a pressure medium. The solidification of this medium occurs around ~6–7 GPa at room temperature[47, 49]. For both cells, the pressure at low temperature was determined by the superconducting transition temperature of Pb[50] measured by the resistivity.

The resistivity measurement under pressure at zero field is described in ref. [16].

Data availability. The data that support the findings of this study are available on request from the corresponding authors.

Received: 4 November 2016 Accepted: 23 June 2017
Published online: 15 September 2017

References

1. Mathur, N. et al. Magnetically mediated superconductivity in heavy fermion compounds. *Nature* **394**, 39–43 (1998).
2. Saxena, S. S. et al. Superconductivity on the border of itinerant-electron ferromagnetism in UGe_2. *Nature* **406**, 587–592 (2000).
3. Aoki, D. et al. Coexistence of superconductivity and ferromagnetism in URhGe. *Nature* **413**, 613–616 (2001).
4. Huy, N. T. et al. Superconductivity on the border of weak itinerant ferromagnetism in UCoGe. *Phys. Rev. Lett.* **99**, 067006 (2007).
5. Brando, M., Belitz, D., Grosche, F. M. & Kirkpatrick, T. R. Metallic quantum ferromagnets. *Rev. Mod. Phys.* **88**, 025006 (2016).
6. Goto, T., Shindo, Y., Takahashi, H. & Ogawa, S. Magnetic properties of the itinerant metamagnetic system $Co(S_{1-x}Se_x)_2$ under high magnetic fields and high pressure. *Phys. Rev. B* **56**, 14019–14028 (1997).
7. Huxley, A. D., Sheikin, I. & Braithwaite, D. Metamagnetic behavior near the quantum critical point in Uge_2. *Physica B* **284**, 1277–1278 (2000).
8. Uhlarz, M., Pfleiderer, C. & Hayden, S. M. Quantum phase transitions in the itinerant ferromagnet $ZrZn_2$. *Phys. Rev. Lett.* **93**, 256404 (2004).
9. Colombier, E., Braithwaite, D., Lapertot, G., Salce, B. & Knebel, G. High-pressure transport and microcalorimetry studies on high quality $YbCu_2Si_2$ single crystals. *Phys. Rev. B* **79**, 245113 (2009).
10. Araki, S. et al. Pressure-temperature-field phase diagram in the ferromagnet U_3P_4. *J. Phys. Soc. Jpn* **84**, 024705 (2015).
11. Shimizu, Y. et al. Unusual strong spin-fluctuation effects around the critical pressure of the itinerant ising-type ferromagnet URhAl. *Phys. Rev. B* **91**, 125115 (2015).
12. Kotegawa, H. et al. Pressure-temperature-magnetic field phase diagram of ferromagnetic Kondo Lattice CeRuPO. *J. Phys. Soc. Jpn* **82**, 123711 (2013).
13. Lengyel, E. et al. Avoided ferromagnetic quantum critical point in CeRuPO. *Phys. Rev. B* **91**, 035130 (2015).
14. Cheng, J.-G. et al. Pressure induced superconductivity on the border of magnetic order in MnP. *Phys. Rev. Lett.* **114**, 117001 (2015).
15. Matsuda, M. et al. Pressure dependence of the magnetic ground states in MnP. *Phys. Rev. B* **93**, 100405 (2016).
16. Taufour, V. et al. Ferromagnetic quantum critical point avoided by the appearance of another magnetic phase in $LaCrGe_3$ under pressure. *Phys. Rev. Lett.* **117**, 037207 (2016).
17. Belitz, D., Kirkpatrick, T. R. & Vojta, T. First order transitions and multicritical points in weak itinerant ferromagnets. *Phys. Rev. Lett.* **82**, 4707–4710 (1999).
18. Sandeman, K. G., Lonzarich, G. G. & Schofield, A. J. Ferromagnetic superconductivity driven by changing Fermi surface topology. *Phys. Rev. Lett.* **90**, 167005 (2003).
19. Chubukov, A. V., Pepin, C. & Rech, J. Instability of the quantum-critical point of itinerant ferromagnets. *Phys. Rev. Lett.* **92**, 147003 (2004).
20. Belitz, D., Kirkpatrick, T. R. & Rollbuhler, J. Tricritical behavior in itinerant quantum ferromagnets. *Phys. Rev. Lett.* **94**, 247205 (2005).
21. Conduit, G. J., Green, A. G. & Simons, B. D. Inhomogeneous phase formation on the border of itinerant ferromagnetism. *Phys. Rev. Lett.* **103**, 207201 (2009).
22. Karahasanovic, U., Krüger, F. & Green, A. G. Quantum order-by-disorder driven phase reconstruction in the vicinity of ferromagnetic quantum critical points. *Phys. Rev. B* **85**, 165111 (2012).
23. Thomson, S. J., Krüger, F. & Green, A. G. Helical glasses near ferromagnetic quantum criticality. *Phys. Rev. B* **87**, 224203 (2013).
24. Pedder, C. J., Krüger, F. & Green, A. G. Resummation of fluctuations near ferromagnetic quantum critical points. *Phys. Rev. B* **88**, 165109 (2013).
25. Wysokinski, M. M., Abram, M. & Spalek, J. Ferromagnetism in Uge_2: A microscopic model. *Phys. Rev. B* **90**, 081114 (2014).
26. Abdul-Jabbar, G. et al. Modulated magnetism in PrPtAl. *Nat. Phys* **11**, 321–327 (2015).
27. Taufour, V., Kaluarachchi, U. S. & Kogan, V. G. Constraints on the merging of the transition lines at the tricritical point in a wing-structure phase diagram. *Phys. Rev. B* **94**, 060410 (2016).
28. Taufour, V., Aoki, D., Knebel, G. & Flouquet, J. Tricritical point and wing structure in the itinerant ferromagnet Uge_2. *Phys. Rev. Lett.* **105**, 217201 (2010).
29. Kotegawa, H., Taufour, V., Aoki, D., Knebel, G. & Flouquet, J. Evolution toward quantum critical end point in Uge_2. *J. Phys. Soc. Jpn* **80**, 083703 (2011).
30. Kabeya, N. et al. Non-fermi liquid state bounded by a possible electronic topological transition in $ZrZn_2$. *J. Phys. Soc. Jpn* **81**, 073706 (2012).
31. Taufour, V., Villaume, A., Aoki, D., Knebel, G. & Flouquet, J. Magnetic field evolution of critical end point in UGe_2. *J. Phys. Conf. Ser.* **273**, 012017 (2011).
32. Kimura, N. et al. de Haas-van Alphen effect in $ZrZn_2$ under pressure: Crossover between two magnetic states. *Phys. Rev. Lett.* **92**, 197002 (2004).
33. Hornreich, R. M., Luban, M. & Shtrikman, S. Critical behavior at the onset of $\vec{k}$-space instability on the λ line. *Phys. Rev. Lett.* **35**, 1678–1681 (1975).
34. Lin, X., Taufour, V., Bud'ko, S. L. & Canfield, P. C. Suppression of ferromagnetism in the $LaV_xCr_{1-x}Ge_3$ system. *Phys. Rev. B* **88**, 094405 (2013).
35. Pfleiderer, C. & Huxley, A. D. Pressure dependence of the magnetization in the ferromagnetic superconductor Uge_2. *Phys. Rev. Lett.* **89**, 147005 (2002).
36. Hardy, F. et al. Two magnetic Gruneisen parameters in the ferromagnetic superconductor Uge_2. *Phys. Rev. B* **80**, 174521 (2009).
37. Palacio Morales, A. et al. Thermoelectric power quantum oscillations in the ferromagnet UGe_2. *Phys. Rev. B* **93**, 155120 (2016).
38 Belitz, D. & Kirkpatrick, T. R. Quantum triple point and quantum critical endpoints in metallic magnets. Preprint at http://arxiv.org/abs/1708.00103 (2017).
39. Aoki, D. et al. Ferromagnetic quantum critical endpoint in UCoAl. *J. Phys. Soc. Jpn* **80**, 094711 (2011).
40. Combier, T., Aoki, D., Knebel, G. & Flouquet, J. Ferromagnetic quantum criticality studied by hall effect measurements in UCoAl. *J. Phys. Soc. Jpn* **82**, 104705 (2013).
41. Kimura, N. et al. Quantum critical point and unusual phase diagram in the itinerant-electron metamagnet UCoAl. *Phys. Rev. B* **92**, 035106 (2015).
42. Wu, W. et al. Quantum critical metamagnetism of $Sr_3Ru_2O_7$ under hydrostatic pressure. *Phys. Rev. B* **83**, 045106 (2011).
43. Canfield, P. C. & Fisk, Z. Growth of single-crystals from metallic fluxes. *Philos. Mag. B-Phys. Condens. Matter Stat. Mech. Electron. Opt. Magn. Prop* **65**, 1117–1123 (1992).
44. Canfield, P. C. & Fisher, I. R. High-temperature solution growth of intermetallic single crystals and quasicrystals. *J. Cryst. Growth.* **225**, 155–161 (2001).
45. Cadogan, J. M., Lemoine, P., Slater, B. R., Mar, A. & Avdeev, M. Neutron diffraction study of the hexagonal perovskite-type compound lacrge3. *Solid State Phenom* **194**, 71–74 (2013).

46. Bud'ko, S. L., Voronovskii, A. N., Gapotchenko, A. G. & Itskevich, E. S. The Fermi surface of cadmium at an electron-topological phase transition under pressure. *Zh. Eksp. Teor. Fiz.* **86**, 778-783 (1984).
47. Torikachvili, M. S., Kim, S. K., Colombier, E., Bud'ko, S. L. & Canfield, P. C. Solidification and loss of hydrostaticity in liquid media used for pressure measurements. *Rev. Sci. Instrum.* **86**, 123904 (2015).
48. Colombier, E. & Braithwaite, D. Simple adaptation of the Bridgman high pressure technique for use with liquid media. *Rev. Sci. Instrum.* **78**, 093903 (2007).
49. Tateiwa, N. & Haga, Y. Evaluations of pressure-transmitting media for cryogenic experiments with diamond anvil cell. *Rev. Sci. Instrum.* **80**, 123901 (2009).
50. Bireckoven, B. & Wittig, J. A diamond anvil cell for the investigation of superconductivity under pressures of up to 50 GPa: Pb as a low temperature manometer. *J. Phys. E: Sci. Instrum* **21**, 841–848 (1988).

Acknowledgements

We would like to thank S.K. Kim, X. Lin, V.G. Kogan, D.K. Finnemore, E.D. Mun, H. Kim, Y. Furukawa, R. Khasanov for useful discussions. This work was carried out at the Iowa State University and the Ames Laboratory, US DOE, under Contract No. DE-AC02-07CH11358. This work was supported by the Materials Sciences Division of the Office of Basic Energy Sciences of the U.S. Department of Energy. V.T. was partly supported by Ames Laboratorys laboratory-directed research and development (LDRD) funding.

Author contributions

V.T. and P.C. initiated this study. U.K., V.T., and P.C. prepared the single crystals. U.K, V.T., and S.B. performed the pressure measurements. U.K., V.T., S.B., and U.K. analyzed and interpreted the pressure data. U.K. and V.T. wrote the manuscript with the help of all authors.

Additional information

Supplementary Information accompanies this paper at doi:10.1038/s41467-017-00699-x.

Competing interests: The authors declare no competing financial interests.

Reprints and permission information is available online at http://npg.nature.com/reprintsandpermissions/

Publisher's note: Springer Nature remains neutral with regard to jurisdictional claims in published maps and institutional affiliations.

Open Access This article is licensed under a Creative Commons Attribution 4.0 International License, which permits use, sharing, adaptation, distribution and reproduction in any medium or format, as long as you give appropriate credit to the original author(s) and the source, provide a link to the Creative Commons license, and indicate if changes were made. The images or other third party material in this article are included in the article's Creative Commons license, unless indicated otherwise in a credit line to the material. If material is not included in the article's Creative Commons license and your intended use is not permitted by statutory regulation or exceeds the permitted use, you will need to obtain permission directly from the copyright holder. To view a copy of this license, visit http://creativecommons.org/licenses/by/4.0/.

© The Author(s) 2017